Synthesis and Structural Characterization of Pyrazole-Bridged Metalla-Bis(dicarbollide) Derivatives of Cobalt, Nickel, Copper, and Iron: Models for Venus Flytrap Cluster Reagents

Aravamuthan Varadarajan, Stephen E. Johnson,[1a] Frank A. Gomez,[1b] Sarmistha Chakrabarti, Carolyn B. Knobler, and M. Frederick Hawthorne*

Contribution from the Department of Chemistry and Biochemistry, University of California at Los Angeles, Los Angeles, California 90024. *Received June 3, 1992*

Abstract: The synthesis and characterization of a family of pyrazole-bridged metallacarborane clusters is described. These species serve as nonradioactive models for the corresponding radio-transition-metal carriers which are potentially useful for the antibody-mediated γ-imaging or β-therapy of tumors (Venus flytrap clusters). Both monofunctional and bifunctional chelate precursors were prepared from the reactions of the anions of pyrazole and 4-carbomethoxypyrazole, respectively, with 2 equiv of *closo*-1,8-$C_2B_9H_{11}$. In each instance, *meso*- and *dl*-isomers of the pyrazole-bridged *nido*-carboranes were obtained. The diastereomers were then converted, in the presence of stoichiometric amounts of aqueous base, to the formal 7,9-bis(dicarbollide) anions. The metal ions Co^{3+}, Ni^{3+}, Cu^{3+}, and Fe^{3+} were incorporated into the unsubstituted pyrazole derivative in aqueous media at pH 12–14, resulting in the mixed *meso*- and *dl*-metallacarborane derivatives of **7**, **8**, **9**, and **10**, respectively. The carbomethoxy pyrazole dicarbollide derivative was complexed with Co^{3+} and $^{57}Co^{3+}$ in a similar manner to produce mixed *meso*- and *dl*-cobaltacarborane derivatives of **11** and **12**, respectively. All diastereomeric metallacarborane derivatives were separated by column chromatography or HPLC techniques and characterized by spectroscopic and electrochemical techniques. The molecular structures of *dl*-Co^{3+} (**7a**), *dl*-Ni^{3+} (**8a**), *meso*-Ni^{3+} (**8b**), *meso*-Cu^{3+} (**9b**), *dl*-Fe^{3+} (**10a**), and *meso*-Co^{3+} (**11b**) have been determined from single-crystal X-ray diffraction experiments, and the structures of the diastereomeric complexes are correlated with ^1H and ^{11}B FT NMR spectra. *dl*-**7a** crystallizes in the monoclinic space group $P2_1/c$ with a = 10.618 (1) Å, b = 13.366 (1) Å, c = 14.326 (2) Å, β = 109.925 (3)°, V = 1901 Å^3, and Z = 4. *dl*-**8a** crystallizes in the orthorhombic space group $Pnma$ with a = 13.6874 (7) Å, b = 15.8587 (8) Å, c = 11.2429 (6) Å, V = 2447 Å^3, and Z = 4. *meso*-**8b** crystallizes in the orthorhombic space group $P2_12_12_1$ with a = 7.2139 (5) Å, b = 13.404 (1) Å, c = 19.768 (2) Å, V = 1908 Å^3, and Z = 4. *meso*-**9b** crystallizes in the orthorhombic space group $P2_12_12_1$ with a = 7.1854 (8) Å, b = 13.434 (2) Å, c = 19.980 (2) Å, V = 1925 Å^3, and Z = 4. *dl*-**10a** crystallizes in the monoclinic space group $P2_1/c$ with a = 10.6926 (5) Å, b = 13.3320 (7) Å, c = 14.3288 (7) Å, β = 110.081 (1)°, V = 1952 Å^3, and Z = 4. *meso*-**11b** crystallizes in the triclinic space group $P\bar{1}$ with a = 9.966 (2) Å, b = 10.475 (2) Å, c = 17.134 (3) Å, α = 79.957 (7)°, β = 77.882 (7)°, γ = 74.732 (7)°, V = 1674 Å^3, and Z = 2. Spectroscopic and structural data for the bridged complexes are compared with those for the corresponding unsubstituted metallacarborane derivatives.

Introduction

The great kinetic stability normally exhibited by metallacarboranes, their inorganic composition, and the ease with which certain classes of them may be prepared from carborane ligands and transition metal ions in aqueous solution prompted our consideration of these species as possible radiometal carriers.[2] Important applications of biologically nondegradable radiometal complexes include their functionalization and subsequent attachment to tumor-targeted monoclonal antibodies for the purposes of tumor diagnosis (γ-emitter) and therapy (β-emitter).[3-5] The existence of strong π-bonding interactions of appropriate transition metal centers with carborane ligands such as the isomeric 7,8-, 7,9-, and 2,9-$C_2B_9H_{11}^{2-}$ dicarbollide ions places *commo*-bis(dicarbollide) transition metal clusters in a class by themselves with regard to chemical stability.[6] The presence of but two carbon vertices per dicarbollide ligand should assure these species of enzymatic invisibility and prevent catabolic degradation in vivo. These characteristics are not available in currently employed radiopharmaceuticals such as the linear and macrocyclic members of the amino carboxylate family (DTPA, DOTA, etc.).[7-15] While clinical use of the latter class of bifunctional chelates is widespread, it appeared to us that a research investment should be made in the design and synthesis of bifunctional radiometal carriers based upon different structural principles; namely functionalized radiometal-containing cluster species.[5] Implementation of this concept using nonradioactive isotopes of the transition metals Co, Cu, Ni, and Fe in a novel pyrazole-bridged *commo*-bis(7,9-dicarbollide) cluster[16] (Venus flytrap cluster, VFC) environment is described herein and in a recently published communication.[17] The corresponding γ-emitting ^{57}Co VFC has been functionalized, conjugated with anti-CEA T84.66 monoclonal antibody, and employed in tumor biodistribution and imaging experiments using athymic female mice bearing LS174T human colon cancer xenografts. These in vivo experiments proved the VFC structure

(1) (a) National Science Foundation Postdoctoral Fellow. (b) National Institute of Health Predoctoral Fellow.
(2) Shelly, K.; Knobler, C. B.; Hawthorne, M. F. *New J. Chem.* **1988**, *12*, 317.
(3) Meares, C. F.; Wensel, T. G. *Acc. Chem. Res.* **1984**, *17*, 202.
(4) Breichbiel, M. W.; Gansow, O. A.; Atcher, R. W.; Schlom, J.; Esteban, J.; Simpson, D. E.; Colcher, D. *Inorg. Chem.* **1986**, *25*, 2772.
(5) Hawthorne, M. F. *Pure Appl. Chem.* **1991**, *63*, 327.
(6) (a) Hawthorne, M. F. *Acc. Chem. Res.* **1968**, *1*, 281. (b) Hawthorne, M. F.; Dunks, G. B. *Science* **1972**, *78*, 462.
(7) Deshpande, S. V.; DeNardo, S. J.; Meares, C. F.; McCall, M. J.; Adams, G. P.; Moi, M. K.; DeNardo, G. L. *J. Nucl. Med.* **1988**, *29*, 217.
(8) Craig, A. S.; Helps, I. M.; Jankowski, K. J.; Parker, D.; Beeley, N. R. A.; Boyce, B. A.; Eaton, M. A. W.; Millican, A. T.; Millar, K.; Phipps, A.; Rhind, S. K.; Harrison, A.; Walker, C. *J. Chem. Soc., Chem. Commun.* **1989**, 794.
(9) Cox, J. P. L.; Jankowski, K. J.; Kataky, R.; Parker, D.; Beeley, N. R. A.; Boyce, B. A.; Eaton, M. A. W.; Millar, K.; Millican, A. T.; Harrison, A.; Walker, C. *J. Chem. Soc., Chem. Commun.* **1989**, 797.
(10) Deshpande, S. V.; DeNardo, S. J.; Kukis, D. J.; Moi, M. K.; McCall, M. J.; DeNardo, G. L.; Meares, C. F. *J. Nucl. Med.* **1990**, *31*, 473.
(11) Greager, J. A.; Chao, T.-C.; Blend, M. J.; Atcher, R. W.; Gansow, O. A.; Brechbiel, M. W.; Das Gupta, T. K. *J. Nucl. Med.* **1990**, *31*, 1378.
(12) Brechbiel, M. W.; Pippin, C. G.; McMurry, T. J.; Milenic, D.; Roselli, M.; Colcher, D.; Gansow, O. A. *J. Chem. Soc., Chem. Commun.* **1991**, 1169.
(13) Mathias, C. J.; Welch, M. J.; Green, M. A.; Diril, H.; Meares, C. F.; Gropler, R. J.; Bergmann, S. R. *J. Nucl. Med.* **1991**, *32*, 475.
(14) Kline, S. T.; Betebrenner, D. A.; Johnson, D. K. *Bioconjugate Chem.* **1991**, *2*, 26.
(15) McMurry, T. J.; Brechbiel, M.; Kumar, K.; Gansow, O. A. *Bioconjugate Chem.* **1992**, *3*, 108.
(16) In order to simplify the discussion and accommodate the bridged structure of ligand systems **3** and **4**, we have employed the older nomenclature style which emphasizes the construction of VFC from dicarbollide ligands, whereas the molecular structures from X-ray analysis are labeled by normal convention.
(17) Hawthorne, M. F.; Varadarajan, A.; Knobler, C. B.; Chakrabarti, S. *J. Am. Chem. Soc.* **1990**, *112*, 5365.

0002-7863/92/1514-9003$03.00/0

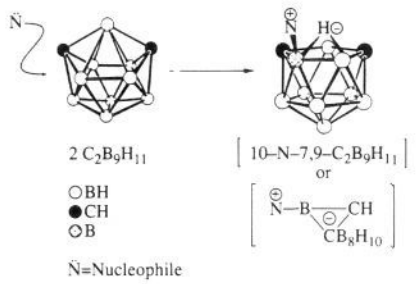

Figure 1. Conversion of *closo*-1,8-$C_2B_9H_{11}$ to the *nido*-10-substituted-7,9-$C_2B_9H_{11}$ zwitterion by nucleophilic attack of a neutral electron donor, N.

Scheme I

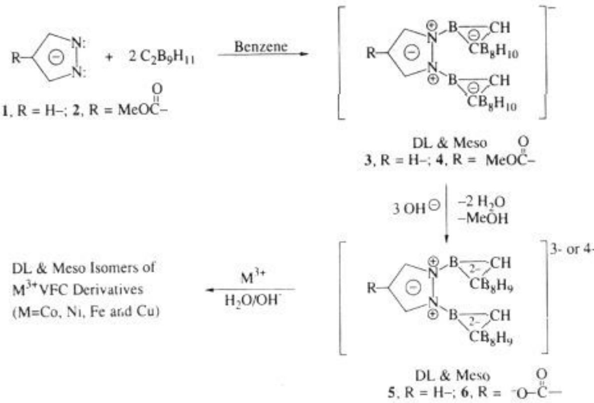

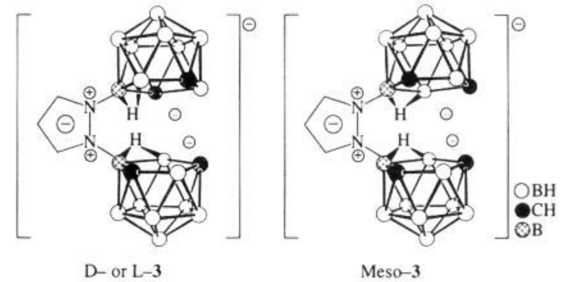

Figure 2. Structures of the *meso*- and *dl*-isomers of 3.

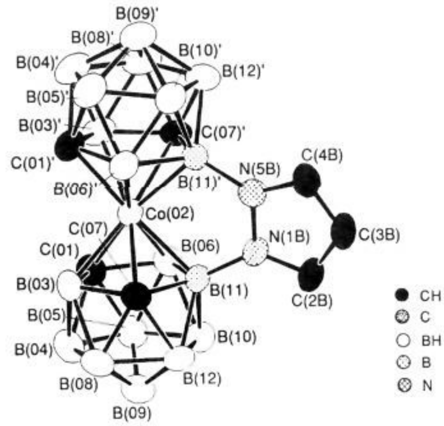

Figure 3. ORTEP representation of **7a** showing the numbering scheme.[16] All hydrogen atoms were removed for clarity. Ellipsoids were drawn at the 0.5 probability level.

to be both resistant to catabolism and apparently excreted intact. The biological results have been reported elsewhere in full.[18] This paper describes the Venus flytrap ligand, its carboxylic acid derivative, and the synthesis, structural characterization, and reactivity of the representative first-row transition metal VFC species enumerated above.

Results

The search for optimization of the kinetic stability inherent in transition metal *commo*-bis(dicarbollide) clusters suggested that the halves of the ligand system should be bridged together.[2] Such a bridge could also carry the functional group required for the attachment of the cluster array to the desired monoclonal antibody or antibody fragment.[3] While bridged *commo*-bis(dicarbollide) species are known which utilize B–E (E = S, N, O) bonds in the cage–bridge connection, these species have only been prepared in the past by modification of the existing *commo*-metallacarborane and the parent ligand systems from which these species are formally derived remain unknown.[19–23] Recent developments toward the synthesis of monofunctional carbon-substituted *closo*-carboranes has led to the synthesis and structural characterization of B–C-bonded, alkylene-bridged *commo*-bis(7,8-dicarbollide) ligands and their conversion to several of their transition metal clusters.[24] These modified VFC structures will be prepared with a radiometal such as ^{57}Co and evaluated with respect to radioimaging and biodistribution experiments.

Pyrazole-Bridged Ligand Syntheses. In the present instance, B–N-bonded pyrazole bridges were employed to connect two 7,9-dicarbollide anions, thus forming two diastereomeric ligand systems, *meso* and *dl*. The assembly of the pyrazole-bridged ligand system was accomplished in a single step by an adaptation of the previously described reaction, shown in Figure 1, which involves the nucleophilic attack of an electron-donor atom upon a boron atom of the *closo*-1,8-$C_2B_9H_{11}$ carborane.[25] Scheme I depicts the 2-fold reaction of the pyrazole dianion (**1**) or its 4-carbomethoxy derivative (**2**) with this reactive carborane. The anionic products of these reactions were isolated in high yield as a roughly 1:1 mixture (NMR) of diastereomeric (*dl*- and *meso*-**3** and *dl*- and *meso*-**4**) triethylammonium salts. The mixture of diastereomers of **3**, as the Me_4N^+ salts, was characterized spectroscopically, by negative ion FAB mass spectrometry and by elemental analyses. The diastereomers of **4** were similarly characterized as the mixed Et_3N^+H salts. Figure 2 depicts the structures of the diastereomers of **3**.

The conversion of the ligand precursors **3** and **4** to their corresponding *commo*-metallacarboranes was accomplished by reaction of the precursors with the desired metal ion in concentrated aqueous base. Under these conditions, the bridged bis(7,9-dicarbollide) ligands **5** and **6** are formally generated in situ by loss of two protons and subsequent capture of the transition metal ion. Aqueous-phase reactions of this type are well documented, and they provide one of the most convenient routes to the simple *commo*-bis(dicarbollide) metallacarboranes of Co, Fe, Ni, Cu, and others.[26] In the case of precursor ion **4**, the methyl ester function was simultaneously hydrolyzed to the carboxylic acid group, which was employed in subsequent antibody conjugation of the ^{57}Co VFC.

Synthesis of Transition Metal Venus Flytrap Clusters. Except in the case of the iron VFC, the transition metal derivatives were

(18) Beatty, B.; Paxton, R. J.; Hawthorne, M. F.; Varadarajan, A.; Williams, L. E.; Curtis, F. L.; Knobler, C. B.; Beatty, J. D.; Shively, J. E. *Proc. Natl. Acad. Sci. U.S.A.* **1991**, *88*, 3387.
(19) Churchill, M. R.; Gold, K.; Francis, J. N.; Hawthorne, M. F. *J. Am. Chem. Soc.* **1969**, *91*, 1222.
(20) Francis, J. N.; Hawthorne, M. F. *Inorg. Chem.* **1971**, *10*, 594.
(21) Francis, J. N.; Jones, C. J.; Hawthorne, M. F. *J. Am. Chem. Soc.* **1972**, *94*, 4878.
(22) Plesek, J.; Hermanek, S.; Base, K.; Todd, L. J.; Wright, W. F. *Collect. Czech. Chem. Commun.* **1976**, *41*, 3509.
(23) Janousek, A.; Plesek, J.; Hermanek, S.; Base, K.; Todd, L. J.; Wright, W. F. *Collect. Czech. Chem. Commun.* **1981**, *46*, 2818.
(24) Gomez, F. A.; Johnson, S. E.; Knobler, C. B.; Hawthorne, M. F. *Inorg. Chem.* **1992**, *31*, 3558.
(25) Tebbe, F. N.; Garrett, P. M.; Hawthorne, M. F. *J. Am. Chem. Soc.* **1968**, *90*, 869.
(26) Hawthorne, M. F.; Young, D. C.; Andrews, T. D.; Howe, D. V.; Pilling, R. L.; Pitts, A. D.; Reintjies, M.; Warren, L. F.; Wegner, P. A. *J. Am. Chem. Soc.* **1968**, *90*, 879.

Table I. Selected Interatomic Distances and Angles for **7a**

Distances (Å)			
Co(02)–B(11′)	2.047 (4)	Co(02)–B(06)	2.089 (4)
Co(02)–B(11)	2.050 (4)	Co(02)–B(06′)	2.095 (4)
Co(02)–C(07)	2.070 (4)	Co(02)–C(01)	2.108 (4)
Co(02)–C(07′)	2.072 (4)	Co(02)–C(01′)	2.118 (4)
Co(02)–B(03)	2.072 (4)	C(01)–B(03)	1.699 (5)
Co(02)–B(03′)	2.074 (4)	C(01)–B(06)	1.691 (6)
B(11′)–N(5B)	1.519 (5)	C(01)–B(04)	1.717 (6)
B(11)–N(1B)	1.523 (5)	C(01)–B(05)	1.729 (6)

Bond Angles (deg)	
B(11)–Co(02)–B(11′)	85.59 (16)
B(06′)–Co(02)–C(07)	90.23 (15)
B(03)–Co(02)–C(01′)	95.50 (17)
B(09)–Co(02)–B(09′)	175.4 (1)

Table II. Selected Interatomic Distances and Angles for **8a**

Distances (Å)			
Ni(02)–C(01)	2.168 (6)	C(01)–B(03)	1.660 (9)
Ni(02)–C(07)	2.137 (6)	C(01)–B(04)	1.726 (10)
Ni(02)–B(03)	2.140 (7)	C(01)–B(05)	1.727 (10)
Ni(02)–B(11)	2.181 (6)	C(01)–B(06)	1.763 (9)
Ni(02)–B(06)	2.079 (7)	B(06)–N(1B)	1.504 (8)

Bond Angles (deg)	
B(06)–Ni(02)–B(06)	85.9 (3)
B(03)–Ni(02)–C(01)	113.1 (2)
C(01)–Ni(02)–B(11)	153.7 (2)
B(09)–Ni(02)–B(09)	173.7 (2)

formed (Scheme I) as a roughly 1:1 mixture of *dl*- (designated as series a) and *meso*- (designated as series b) isomers. The iron VFC complex isolated by conventional column chromatography in 43% yield proved to be the enantiomeric *dl*-species **10a**. No explanation for this observation can be offered at this time. The Co (**7ab**), Ni (**8ab**), and Cu (**9ab**) VFC species were successfully separated into their component *dl*- and *meso*-isomers by HPLC, and these pure species were characterized by NMR, IR, and FAB MS methods and structurally defined by X-ray diffraction studies. Elemental analyses and cyclic voltammetry measurements were obtained with purified diastereomeric mixtures.

Interest in a very stable d^6 radiotransition metal VFC antibody conjugate capable of tumor imaging predicated this effort and suggested ^{57}Co (γ, $t_{1/2}$ = 270 d) as a desirable isotope of cobalt for initial biological study. Previous chemical, radiochemical, and biological results have been reported,[17,18] and we here present the syntheses of the isotopically normal cobalt derivatives of ligand precursors **3** and **4**, **7ab** and **11ab**, respectively, as well as the metallation and antibody conjugation procedure employed with ^{57}Co-VFC-COOH (**12ab**) (vide infra).

Structural Studies. The Co VFC was obtained as a mixture of diastereomers **7ab** in 48% yield. The structure of **7a** was determined by X-ray diffraction and is presented in Figure 3. Selected bond distances and angles are presented in Table I, while the atomic positional coordinates are provided in the supplementary material along with thermal parameters, hydrogen atom parameters, and additional bond lengths and angles. Species **7a** is clearly established as the *dl*-diastereomer. Each of the bonding faces of the component 7,9-dicarbollide ligands is planar to within 0.068 (5) Å, and Co distances to these planes are 1.482 (1) Å (unprimed atoms) and 1.489 (1) Å (primed atoms). Due to the tight bridging of the planar pyrazole moiety, the bonding faces of the dicarbollide ligands are eclipsed. The angle between normals to the two bonding planes is 6.6 (1)°, Co–C distances range from 2.070 (4) to 2.118 (4) Å, and Co–B bond interactions range from 2.047 (4) to 2.095 (4) Å. The angle B(09)–Co–B(09′) is 175.4 (1)°. The restriction of rotation of the component dicarbollide ligands and the compression of their bridged edges by the pyrazole bridge is clearly apparent.

The Ni VFC product mixture **8ab** was obtained in 39% yield and resolved into its component paramagnetic diastereomers by HPLC. The structure **8a**, determined by X-ray diffraction, is presented in Figure 4. Selected bond distances and angles are

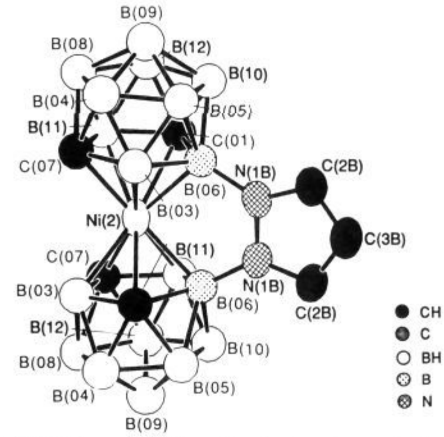

Figure 4. ORTEP representation of **8a** showing the numbering scheme.[16] All hydrogen atoms were removed for clarity. Ellipsoids were drawn at the 0.5 probability level.

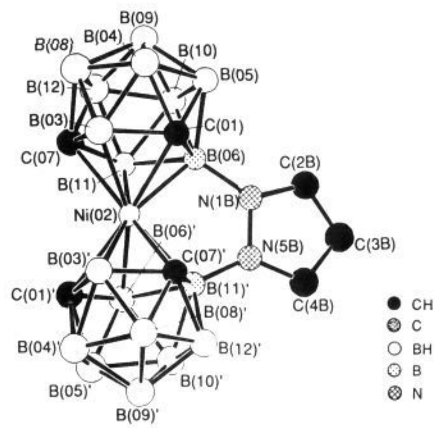

Figure 5. ORTEP representation of **8b** showing the numbering scheme.[16] All hydrogen atoms were removed for clarity. Ellipsoids were drawn at the 0.5 probability level.

Table III. Selected Interatomic Distances and Angles for **8b**

Distances (Å)			
Ni(02)–B(11′)	2.090 (6)	Ni(02)–C(01)	2.166 (5)
Ni(02)–B(06)	2.104 (6)	Ni(02)–C(01′)	2.187 (5)
Ni(02)–B(03)	2.126 (7)	C(01)–B(03)	1.732 (9)
Ni(02)–B(06′)	2.132 (7)	C(01)–B(06)	1.678 (8)
Ni(02)–B(11)	2.133 (6)	C(07)–B(11)	1.668 (8)
Ni(02)–B(03′)	2.144 (7)	C(07)–B(03)	1.727 (9)
Ni(02)–C(07′)	2.165 (6)	B(06)–N(1B)	1.507 (7)
Ni(02)–C(07)	2.192 (5)	B(11′)–N(5B)	1.514 (8)

Bond Angles (deg)	
B(06)–Ni(02)–B(11′)	85.21 (24)
C(01)–Ni(02)–C(07′)	92.64 (21)
B(11)–Ni(02)–B(06′)	90.84 (24)
B(09)–Ni(02)–B(09′)	171.9 (1)

presented in Table II, and atomic coordinates, thermal parameters, and additional bond lengths and angles are provided as supplementary material. The bonding faces of the eclipsed dicarbollide components are planar to within 0.049 (7) Å, and Ni distances to these planes are 1.568 (1) Å (molecular symmetry causes the dicarbollide bonding faces to be equivalent). The angle between normals to the two bonding faces is 8.0 (5)°. The Ni–C distances range from 2.137 (6) to 2.168 (6) Å, and Ni–B contacts range from 2.079 (7) to 2.181 (6) Å. The B(09)–Ni–B(09) angle is 173.7 (2) Å. The two dicarbollide moieties are compressed toward each other at the pyrazole bridge juncture. The structure of the *meso*-isomer (**8b**) is presented in Figure 5. Table III presents selected bond distances and angles. The supplementary material contains the atomic coordinates, thermal parameters, hydrogen atom parameters, and additional bond lengths and angles. Each

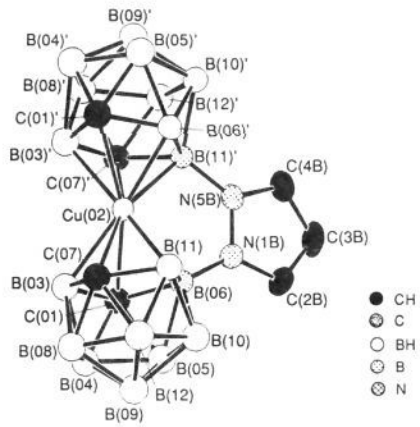

Figure 6. ORTEP representation of **9b** showing the numbering scheme.[16] All hydrogen atoms were removed for clarity. Ellipsoids were drawn at the 0.5 probability level.

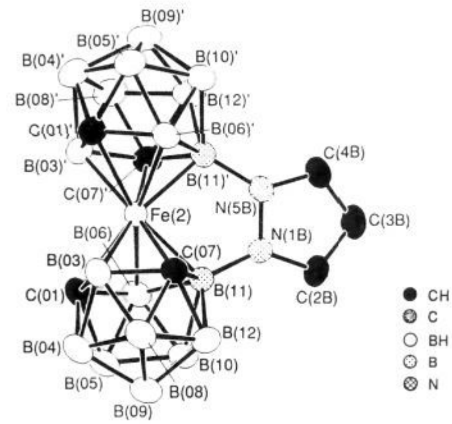

Figure 7. ORTEP representation of **10a** showing the numbering scheme.[16] All hydrogen atoms were removed for clarity. Ellipsoids were drawn at the 0.5 probability level.

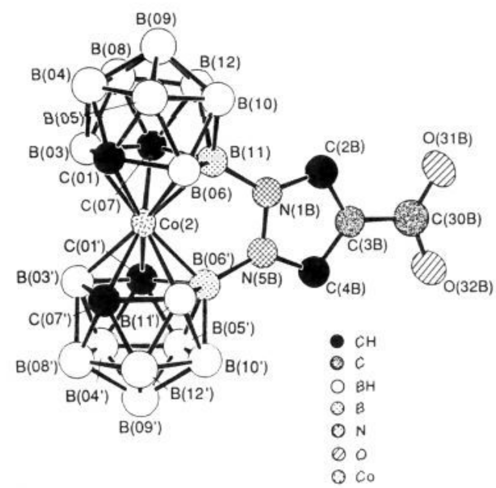

Figure 8. ORTEP representation of **11b** showing the numbering scheme.[16] All hydrogen atoms were removed for clarity. Ellipsoids were drawn at the 0.5 probability level.

Table IV. Selected Interatomic Distances and Angles for **9b**

Distances (Å)			
Cu(02)-B(06′)	2.169 (6)	Cu(02)-Cu(07)	2.223 (5)
Cu(02)-B(11)	2.136 (6)	Cu(02)-Cu(07′)	2.304 (5)
Cu(02)-B(11′)	2.153 (6)	C(01)-B(06)	1.656 (8)
Cu(02)-B(03′)	2.154 (7)	C(01)-B(04)	1.667 (9)
Cu(02)-B(06)	2.158 (6)	C(07)-B(11)	1.653 (8)
Cu(02)-B(03)	2.182 (7)	C(07)-B(03)	1.692 (9)
Cu(02)-C(01′)	2.257 (5)	B(06)-N(1B)	1.518 (7)
Cu(02)-C(01)	2.349 (6)	B(11′)-N(5B)	1.516 (7)

Bond Angles (deg)	
B(06)-Cu(02)-B(11′)	84.76 (22)
B(06′)-Cu(02)-B(11)	96.71 (24)
C(01)-Cu(02)-C(07′)	113.23 (21)
B(09)-Cu(02)-B(09′)	167.4 (2)

Table V. Selected Interatomic Distances and Angles for **10a**

Distances (Å)			
Fe(2)-C(01)	2.149 (2)	Fe(2)-C(07′)	2.086 (2)
Fe(2)-B(03)	2.124 (3)	Fe(2)-B(11′)	2.055 (2)
Fe(2)-B(06)	2.117 (3)	C(01)-B(03)	1.682 (3)
Fe(2)-C(07)	2.090 (2)	C(01)-B(06)	1.686 (3)
Fe(2)-B(11)	2.057 (3)	C(07)-B(03)	1.689 (3)
Fe(2)-C(01′)	2.157 (2)	C(07)-B(11)	1.697 (3)
Fe(2)-B(03′)	2.119 (3)	B(11)-N(1B)	1.518 (3)
Fe(2)-B(06′)	2.114 (2)	B(11′)-N(5B)	1.513 (3)

Bond Angles (deg)	
B(11)-Fe(2)-B(11′)	85.2 (1)
C(07)-Fe(2)-B(06′)	91.5 (1)
B(06)-Fe(2)-C(07′)	91.6 (1)
B(09)-Fe(2)-B(09′)	173.5 (1)

Table VI. Selected Interatomic Distances and Angles for **11b**

Distances (Å)			
Co(2)-C(01)	2.085 (9)	C(01)-B(06)	1.694 (14)
Co(2)-C(07)	2.061 (8)	C(01)-B(03)	1.689 (14)
Co(2)-B(03′)	2.103 (11)	C(07)-B(03)	1.702 (13)
Co(2)-B(08′)	2.039 (10)	C(07)-B(11)	1.706 (13)
Co(2)-B(03)	2.087 (11)	B(11)-N(1B)	1.538 (12)
Co(2)-B(06)	2.080 (11)	B(08′)-N(5B)	1.517 (12)
Co(2)-B(06′)	2.072 (11)		
Co(2)-B(11)	2.034 (10)		
Co(2)-C(01′)	2.077 (9)		
Co(2)-C(07′)	2.056 (8)		

Bond Angles (deg)	
B(11)-Co(02)-B(08′)	85.4 (4)
B(06)-Co(02)-B(03′)	86.4 (4)
C(07)-Co(02)-C(07′)	92.1 (3)
B(09)-Co(02)-B(09′)	175.1 (2)

of the dicarbollide bonding faces is planar to within 0.099 (7) Å, and Ni distances to these planes are 1.570 (1) Å (unprimed atoms) and 1.575 (1) Å (primed atoms). The bonding faces are eclipsed, and the angle between normals to these faces is 10.4 (3)°. The Ni-C distances range from 2.165 (6) to 2.192 (5) Å, and Ni-B distances vary from 2.090 (6) to 2.144 (7) Å. The B(09)-Ni-B(09′) angle is 171.9 (1)°.

The diamagnetic Cu VFC isomer mixture **9ab** was obtained in 42% yield. Separation of **9a** and **9b** provided crystals of **9b** suitable for an X-ray diffraction study. The structure of **9b** is presented in Figure 6. Table IV presents selected bond distances and angles. The supplementary material contains the atomic coordinates, thermal parameters, hydrogen atom parameters, and additional bond distances and angles. Each of the bonding faces of the dicarbollide structural components is planar to within 0.123 (7) Å, and Cu distances to these planes are 1.670 (2) Å (unprimed atoms) and 1.664 (2) Å (primed atoms). The dicarbollide bonding faces are eclipsed, and the angle between normals to these faces is 14.1 (3)°. The Cu-C distances vary from 2.223 (5) to 2.349 (6) Å, and Cu-B interactions range from 2.136 (6) to 2.182 (7) Å. The B(09)-Cu-B(09′) angle is 167.4 (2)°.

As pointed out above, only the *dl*-diastereomer of the Fe VFC (**10a**) was isolated, in 43% yield. The molecular structure of **10a** is presented in Figure 7. Table V provides selected bond distances and angles, while the supplementary material provides atomic positional coordinates, thermal parameters, hydrogen atom parameters, and additional bond lengths and angles. The dicarbollide bonding faces are coplanar to within 0.061 (3) Å, and the Fe distances to these planes are 1.526 (3) Å (unprimed atoms) and 1.529 (3) Å (primed atoms). The angle between normals to the eclipsed bonding faces is 9.6 (2)°. The Fe-C distances range from 2.086 (2) to 2.157 (2) Å, while the Fe-B interactions vary from

Table VII. Reduction Potentials for M^{3+} VFC and Related *commo*-Bis(7,9-dicarbollide) Derivatives

compound	solvent	$E_{1/2}$ vs SCE			ref
		M^{IV}/M^{III}	$M^{III/II}$	$M^{II/I}$	
Fe VFC (**10ab**)	acetonitrile[a]		+0.30		this work
Co VFC (**7ab**)	acetonitrile[a]		−0.59	−1.80	this work
Ni VFC (**8ab**)	acetonitrile[a]	1.56	−0.19	−1.76	this work
Cu VFC (**9ab**)	acetonitrile[a]		−0.08	−0.72	this work
$[Cs](7,9-C_2B_9H_{11})_2Co]$	acetone[b]	irrev	−1.17		26
$[Et_4N][(7,9-C_2B_9H_{11})_2Co]$	acetonitrile[c]		−1.14	−2.52	34
$[Et_4][(7,9-C_2B_9H_{11})_2Ni]$	acetonitrile[c]		−0.92	−2.09	34
$[(7,9-C_2B_9H_{11})_2Ni]$	acetonitrile[c]	0.55	−0.91		26

[a] 0.1 M Bu_4NPF_6 supporting electrolyte. [b] 50% aqueous acetone, 0.1 N $LiClO_4$ supporting electrolyte. [c] 0.1 N Et_4NClO_4 supporting electrolyte.

2.055 (2) to 2.124 (3) Å. The B(09)–Fe–B(09′) angle is 173.5 (1)°.

The functionalized VFC derivative Co-VFC-COOH (**11ab**) was obtained in 50% yield. Separation of the 1:1 mixture of diastereomers provided the *meso*-isomer (**11b**) suitable for an X-ray diffraction study. The structure of **11b** is presented in Figure 8. Selected bond distances and angles are given in Table VI, and the supplementary material contains atomic coordinates, thermal parameters, hydrogen atom parameters, and additional bond distances and angles. Each of the bonding faces of the dicarbollide components are coplanar to within 0.07 (1) Å, and Co distances to these planes are 1.478 (1) Å (unprimed atoms) and 1.475 (1) Å (primed atoms). The angle between the normals of the eclipsed bonding faces is 6.2 (9)°. The Co–C distances range from 2.056 (8) to 2.085 (9) Å, while the Co–B contacts vary from 2.034 (10) to 2.103 (11) Å. The B(09)–Co–B(09′) angle is 175.1 (2)°.

Electrochemical Studies. The results of cyclic voltammetry experiments with the unsubstituted VFC derivatives [μ-$C_3N_2H_3$-$(7,9-C_2B_9H_{10})_2M$] are summarized in Table VII. For M = Co, Ni, Cu, and Fe, plots of $v^{1/2}$ vs i are linear for each of the reductions, indicating electrochemical reversibility for these processes. The Fe^{3+} derivative undergoes a single one-electron reduction, while the Co^{3+} and Cu^{3+} derivatives undergo two one-electron reductions. The nickel VFC species exhibit three reduction waves, consistent with Ni(I/II), Ni(II/III), and Ni(III/IV) redox couples. Within experimental error, the diastereomeric VFC M^{III} derivatives exhibited the same redox potentials. Due to the difference in ionic charge between VFC species and the corresponding *commo*-bis(7,9-dicarbollide) complexes, no direct comparison of electrochemical data is possible, since all the VFC complexes are more easily reduced.

NMR Studies. The Fe^{3+} and Ni^{3+} VFC derivatives exhibited paramagnetic ^1H and ^{11}B NMR spectra, consistent with their respective d^5 and d^7 electron configurations, respectively. In addition, the ^{11}B NMR spectra contained no evidence of spin–spin coupling of the ^{11}B nuclei with the hydrogen to which they are bonded. The range of paramagnetic ^1H and ^{11}B NMR contact shifts decreased in the order $Fe^{3+} > Ni^{3+}$. The Co^{3+} VFC complexes exhibited characteristic diamagnetic ^1H and ^{11}B NMR spectra in agreement with the d^6 configuration of Co(III) as did the d^8 Cu(III) VFC complexes.[26]

Bioconjugation and Tumor Imaging. The preparation of the ^{57}Co VFC was similar to that of the nonradiolabeled derivative (Scheme I), only on a much smaller scale. $^{57}CoCl_2$ was incorporated into the VFC ligand (present in a large excess). The basic conditions also facilitated removal of the protecting group in the pyrazole carboxyl function, which was subsequently utilized for conjugation to antibody. Acidification and extraction from ether afforded ^{57}Co VFC with a radiochemical yield of 59%. Studies using nonradiolabeled $CoCl_2$ have shown that the ether-extracted product is essentially pure, because excess ligand and reaction byproducts are insoluble in ether. Anti-carcinoembryonic antigen (CEA) mAb T84.66[27,28] was used for radiolabeling with **12ab**. Conversion of the mixture of diastereomeric **11ab** species to their active *N*-hydroxysulfosuccinimide esters was carried out by using 1-ethyl-3-[3-(dimethylamino)propyl]carbodiimide in acetonitrile, and the diastereomeric product mixture was purified by reverse-phase HPLC using a C_8 column (62% yield). High conjugation yields were achieved with the active esters of **11ab** and model lysine-containing peptides. The reaction of the active esters derived from **12ab** which contained radioactive ^{57}Co ($t_{1/2}$ = 271 days, γ-emission) with the anti-carcinoembryonic antigen mAb produced a conjugate which carried, on the average, 0.05 $^{57}Co^{3+}$ VFCs per mAb molecule after purification by HPLC. The conjugated mAb retained >90% of its original immunoreactivity by enzyme immunoassay. The tumor-targeting properties of the antibody conjugate were evaluated in nude mice with human colon tumor xenografts over a period of 168 h.[9] Excellent γ-imaging was attained, and biodistribution studies showed a steady increase in both tumor/liver (T/L) and tumor/blood (T/B) ratios with time (T/L and T/B were respectively 2.88 and 1.21 at t = 48 h and 3.48 and 1.40 at t = 168 h). The results of imaging and biodistribution experiments are presented in detail elsewhere.[17,18]

Discussion

The search for exceptionally stable molecular structures with which to bind radioisotopes for purposes of radioimaging (γ-emitters) and therapy (β-emitters) was recently extended to pyrazole-bridged radiometallacarboranes in the instance of a ^{57}Co (122.1 and 136.5 keV, γ, $t_{1/2}$ = 271 d) VFC (**12**) conjugated with an effective antitumor monoclonal antibody. As expected, this radioactive inorganic cluster moiety remained viable in vivo for very long periods of time and was apparently excreted in feces as a metallacarborane derivative accompanying the normal discharge of bile into the duodenum.[18] This remarkable resistance to catabolism by an inorganic structure suggests the extension of VFC–monoclonal antibody conjugates to include other radiotransition metals for diagnostic or therapeutic purposes. Such candidate radiometals include ^{66}Ni, β^-, 55 h; ^{67}Cu, β^-, 62 h; ^{99m}Tc, γ, 6 h; ^{105}Rh, β^-, 35 h; ^{186}Re, β^-, 9 h; and ^{188}Re, β^-, γ, 17 h. In the work reported here, we have restricted the selection of metals for VFC modeling purposes to those of the latter half of the first-row transition metal series: Fe, Co, Ni, and Cu. These metals were previously placed in well-characterized *commo*-bis(7,8-dicarbollide) and *commo*-bis(7,9-dicarbollide) clusters.[26,29-33]

The two-nitrogen atom bridge provided by the pyrazole molecule which is B–N bonded to the two η^5-7,9-dicarbollide ligands of the VFC species strongly influences the structural characteristics of these compounds. Thus, the two 7,9-dicarbollide ligands which constitute the commo cluster structure of these VFC species are forced into eclipsed conformations regardless of the *dl* or *meso* stereochemistry of the VFC. Furthermore the η^5-faces of the 7,9-dicarbollide components are tilted with respect to each other because they are linked by the short N–N bond of the pyrazole bridge. This tilt is exaggerated in the case of the formal d^8

(27) Wagener, C.; Yang, Y. H.; Crawford, F. G.; Shively, J. E. *J. Immunol.* **1983**, *130*, 2308.
(28) Wagener, C.; Clark, B. R.; Rickard, K. J.; Shively, J. E. *J. Immunol.* **1983**, *130*, 2302.
(29) Warren, L. F.; Hawthorne, M. F. *J. Am. Chem. Soc.* **1968**, *90*, 4823.
(30) Warren, L. F.; Hawthorne, M. F. *J. Am. Chem. Soc.* **1970**, *92*, 1157.
(31) Zalkin, A.; Hopkins, T. E.; Templeton, D. H. *Inorg. Chem.* **1967**, *6*, 1911.
(32) Wing, R. M. *J. Am. Chem. Soc.* **1968**, *90*, 4828.
(33) Kang, H. C.; Lee, S. S.; Knobler, C. B.; Hawthorne, M. F. *Inorg. Chem.* **1991**, *30*, 2024.

meso-Cu^{3+}-VFC (**9b**). The normals to the faces of the two 7,9-dicarbollide fragments form an angle of about 13°. This could be compared with the case of the formal d^6 *meso*-Co^{3+}-VFC-COOH (**11b**) with a corresponding angle of about 6°. This larger tilt distortion seen in the Cu^{3+} VFC may be attributed to the larger effective radius of the sequestered copper center, since the Cu–C and Cu–B distances in **9b** are consistently longer than the corresponding distances in **11b**. The diamagnetic Co^{3+} VFC derivatives, with a formal d^6 electron configuration, all exhibited spectral and redox properties which paralleled those of the corresponding *commo*-bis(7,9-dicarbollide) species. In a similar fashion, the paramagnetic formal d^5 Fe^{3+} and d^7 Ni^{3+} VFC derivatives resembled their corresponding metallacarborane counterparts. Compared to the literature values[26,29,34,35] of $E_{1/2}$ for the cobalt and nickel $M^{III/II}$ redox couples (Table VII), the one additional unit of positive charge associated with the VFC species results in their more facile reduction when compared with the corresponding case of the *commo*-bis(7,9-dicarbollide) complexes.

Conclusions

The results reported here extend the demonstrated applicability of VFC bonding to several additional first-row transition metals. Additional investigations of this sort are in progress both with the original VFC ligand system reported here and with other ligands bridged by functionalized carbon chains anchored to carborane cage carbon vertices. These investigations of more sophisticated VFC models and their biodistributions, tumor-imaging capabilities after mAb conjugation, and in vivo stabilities will be reported elsewhere.

Experimental Section

General Considerations. Standard glovebox, Schlenk, and vacuum line techniques were employed for all manipulations of air- and moisture-sensitive compounds. Reaction solvents were reagent grade and were distilled from appropriate drying agents under nitrogen before use. Tetrahydrofuran and diethyl ether were distilled from sodium benzophenone ketyl; benzene was distilled from potassium benzophenone ketyl. Deuteriated solvents were obtained from Cambridge Isotope Laboratories. All microanalyses were performed by Galbraith Laboratories Inc., Knoxville, TN. Sodium hydride and pyrazole (Aldrich) were used as received. Cobalt chloride, copper chloride (Cerac), nickel bromide (Aldrich), and iron chloride (Alfa) were obtained in argon-filled vessels and were used without further purification. *closo*-1,8-$C_2B_9H_{11}$ and 4-carbomethoxypyrazole were prepared according to literature methods.[25]

Physical Measurements. Proton (^1H NMR) and carbon (^{13}C NMR) spectra were obtained on a Bruker AF 200 at 200.133 and 50.324 MHz, respectively. Boron (^{11}B NMR) spectra were obtained at 160.46 MHz on a Bruker AM 500 spectrometer. Chemical shifts for ^1H and ^{13}C NMR spectra were referenced to $SiMe_4$ and measured with respect to residual protons in deuteriated solvents. Chemical shift values for ^{11}B spectra were referenced relative to external $BF_3{\cdot}OEt_2$. Resonances observed upfield of the references were assigned negative chemical shift values in all cases. Infrared spectra were obtained as Nujol mulls and were recorded on a Beckman FT-1100 instrument. Electron impact mass spectra were obtained on an AEI Ltd. Model MS-902 sector filled double-focusing spectrometer, and xenon FAB mass spectra were obtained on an AEI Ltd. Model MS-9 spectrometer. Cyclic voltammetry was performed with an EG&G (Princeton Applied Research) 362 electrochemical analyzer. All the electrochemical measurements were carried out at room temperature under a nitrogen atmosphere with CH_3CN solutions of the complexes in 0.1 M Bu_4NPF_6 (TBAHP) as a supporting electrolyte. Potentials are refereced to a Ag/AgCl electrode. A glassy carbon electrode and platinum wire were used as the working electrode and auxiliary electrode, respectively.

Preparation of *dl*- and *meso*-Triethylammonium 3. To a suspension of 1.5 equiv of NaH (0.644 g, 26.8 mmol) in dry benzene (60 mL) at 0 °C was added 1.0 equiv of pyrazole in 35 mL benzene (1.22 g, 17.9 mmol) dropwise with stirring. The mixture was allowed to stir for 2 h, maintaining this temperature. After a brisk effervescence had subsided, 2 equiv of *closo*-1,8-$C_2B_9H_{11}$ (4.74 g, 35.8 mmol) in dry benzene (85 mL) was slowly added to the mixture with stirring at 0 °C. The mixture was stirred further for a period of 24 h. The excess NaH was quenched by careful addition of methanol, and the solvent was removed by rotary evaporation. Drying under vacuum produced a white solid which was dissolved in water, and this solution was filtered. Addition of a solution of triethylammonium chloride (2.46 g) in water (75 mL) precipitated the triethylammonium salt of **3** as a roughly 1:1 mixture of diastereomers, which was filtered and dried under vacuum overnight. The solid was redissolved in acetonitrile, and the resulting solution was filtered. Concentration of the filtrate yielded the ligand as a fluffy, white solid, 7.31 g (94% yield). The material was recrystallized from an acetonitrile/water mixture to give colorless crystals, mp 118–121 °C dec. ^1H NMR (CD_3CN) δ: 1.28 (t, 9 H, CH_3/$NHEt_3$), 0.800–2.12 (br peaks, 18 H, Cb B–H), 1.95 (br m, 4 H, Cb C–H), 3.15 (q, 6 H, $-CH_2-$/$NHEt_3$), 4.00–4.16 (br s, 1 H, NH/$NHEt_3$), 6.40 (t, 1 H, pz H), 8.03 (d of d, 2 H, pz H). ^{13}C NMR (acetonitrile) δ: 9.15 (s, CH_3/$NHEt_3$), 35.0, 37.2 (br s, Cb C–H), 47.8 (s, $-CH_2-$/$NHEt_3$), 107.5, 107.6 (s, pz C), 144.7, 144.9 (s, pz C). ^{11}B NMR (acetonitrile) δ: −2.43 (d, 2 B), −3.91 (d, 2 B), −4.98 (d, 2 B), −11.9 (s, 1 B–N), −12.7 (s, 1 B–N), −19.0 (d, 2 B), −20.8 (d, 2 B), −23.5 (d, 2 B), −33.6 (d, 4 B). IR (nujol, cm^{-1}): 3199 (ν_{N-H}), 2528 (ν_{B-H}), 1698 ($\nu_{C=O}$). Negative ion FAB mass spectrum $C_{13}B_{18}H_{41}N_3$ (mass frag, center of envelope *m/e*): M^- 330.45. Calcd for M^-: 331.92. For elemental analysis, the tetramethylammonium derivative was prepared. The material was recrystallized from an acetonitrile/water mixture to give colorless crystals, mp 194–196 °C dec. ^1H NMR (CD_3CN) δ: 2.17 (s, 12 H, NMe_4), 0.885–2.04 (br peaks, 18 H, Cb B–H), 1.90 (br s, 4 H, Cb C–H), 6.16 (t, 1 H, pz H), 7.80 (d of d, 2 H, pz H). ^{11}B NMR (acetonitrile) δ: −2.53 (d, 2 B), −4.05 (d, 2 B), −5.19 (d, 2 B), −12.1 (d, 1 B–N), −12.9 (d, 1 B–N), −19.2 (d, 2 B), −20.8 (d, 2 B), −23.6 (d, 2 B), −33.7 (d, 4 B). IR (nujol, cm^{-1}): 3199 (ν_{N-H}), 2528 (ν_{B-H}), 1698 ($\nu_{C=O}$). Negative ion FAB mass spectrum $C_{11}B_{18}H_{37}N_3$ (mass frag, center of envelope *m/e*): M^-, 331.04. Calcd for M^-: 331.92. Anal. Calcd for $C_{11}B_{18}H_{37}N_3$: C, 32.54; H, 9.19; B, 47.92; N, 10.35. Found: C, 32.57; H, 9.14; B, 47.54; N, 10.35.

Preparation of *dl*- and *meso*-Triethylammonium 4. To a suspension of NaH (0.048 g, 2.00 mmol) in dry THF (10 mL) at ambient temperature was added a solution of 4-carboxypyrazole methyl ester (0.252 g, 2.00 mmol) dropwise with stirring. The mixture was allowed to stir for 30 min at ambient temperature. After a brisk effervescence had subsided, the mixture was stirred overnight. The solvent was removed in vacuo, benzene (25 mL) was added to the dry solid, and the mixture was stirred. Addition of a solution of *closo*-1,8-$C_2B_9H_{11}$ (0.528 g, 4.00 mmol) in dry benzene (75 mL) was followed by stirring overnight at ambient temperature. Dry ether (60 mL) was added, and the mixture was stirred for a further period of 24 h. The excess NaH was quenched by careful addition of methanol, and the solvent was removed by rotary evaporation. Drying under vacuum produced a white solid which was dissolved in water, and this solution was filtered. Addition of a solution of triethylammonium chloride (5.00 g) in water (75 mL) precipitated the triethylammonium salt of **4** as a roughly 1:1 mixture of diastereomers, which was filtered off and dried under vacuum overnight. The solid was redissolved in acetone, and the resulting solution was filtered. Concentration of the filtrate yielded the ligand as a fluffy, white solid. The crude product, weighing 0.900 g (100% yield), was transferred to a separatory funnel and diluted with 200 mL of diethyl ether. The layers were separated, and the aqueous layer was extracted with additional Et_2O (2 × 200 mL). The combined filtrates were then dried over anhydrous $MgSO_4$ and evaporated to dryness. The crude white solids were washed with petroleum ether, and the insoluble solids were collected in 70% yield. ^1H NMR (CD_3OD) δ: 1.74 (br s, 2 H, Cb C–H), 2.90 (s, 18 H, NMe_3), 3.86 (s, 3 H, $COOCH_3$), 8.35 (s, 1 H, pz H), 8.41 (s, 1 H, pz H). ^{11}B NMR (acetone) δ: −2.52 (d, 2 B), −3.87 (d, 2 B), −4.83 (d, 4 B), −12.5 (B–N), −13.3 (B–N), −19.06 (d, 2 B), −21.2 (d, 2 B), −23.42 (d, 2 B), −33.81 (d, 2 B). IR (nujol, cm^{-1}): 3200 (ν_{N-H}), 2527 (ν_{B-H}), 1710 ($\nu_{C=O}$). Negative ion FAB mass spectrum $C_9B_{18}H_{27}N_2O_2$ (mass frag, center of envelope *m/e*): M^-, 391.1. Calcd for M^-: 393.0. The sodium salt of the ligand was prepared by ion-exchange chromatography on Bio Rad AG50W cation-exchange resin (Na^+ form, 20–50 mesh) using a 60:40 acetone/water mixture as the eluate. The eluate was concentrated, filtered, and dried under vacuum to yield the sodium salt as a white solid. Due to its hygroscopic nature, the sodium salt was stored in a vacuum desiccator.

Preparation of *dl*- and *meso*-[μ-$C_3N_2H_3$-(7,9-$C_2B_9H_{10}$)$_2$Co] (7). A basic solution of $CoCl_2$ (0.50 g, 2.10 mmol) in Na_2CO_3 was prepared by addition of the metal complex to a saturated solution of sodium carbonate (35 mL) and by adjusting the pH to 14 by addition of NaOH pellets. The sodium salt of **3** (0.61 g, 1.41 mmol) was added, and the reaction mixture was stirred vigorously at 100 °C overnight. A dark yellow solution formed and persisted upon cooling the reaction to ambient temperature. The mixture was acidified with HCl to neutralize the base, and the cobalt complex was extracted in 4 × 20 mL portions of ether. The ether layer was washed with 4 × 20 mL portions of water, and the

(34) Geiger, W. E.; Smith, D. E. *J. Chem. Soc., Chem. Commun.* **1971**, 8.

(35) Geiger, W. E.; Smith, D. E. *J. Electroanal. Chem. Interfacial Electrochem.* **1974**, *50*, 31.

combined ether washings were dried over anhydrous Na_2SO_4. The ether solvent was removed in vacuo to result in 263.5 mg (48% yield) of yellow-orange, crystalline **7**. The product was obtained as a roughly 1:1 mixture of diastereomers and was recrystallized from CH_2Cl_2. The diastereomers could be separated to yield the orange-brown *dl*-isomer (**7a**) and orange-yellow *meso*-isomer (**7b**) by preparative TLC techniques or by column chromatography using silica gel (5 × 18 cm column) and a benzene/petroleum ether mixture as the eluate. Both isomers could be recrystallized from methylene chloride. Crystals of **7a** suitable for an X-ray diffraction experiment were grown by slow evaporation of concentrated methylene chloride solution, mp 300–300.5 °C. Anal. Calcd for $C_7B_{18}H_{23}N_2Co$: C, 21.62; H, 5.96; B, 50.05; N, 7.21; Co, 15.16. Found: C, 21.30; H, 6.15; B, 49.09; N, 7.39; Co, 14.82. FAB mass spectrum (mass frag, center of envelope m/e): M^+, 387.91. Calcd for M^+: 388.83. *dl*-**7a** ^{1}H NMR ($CDCl_3$) δ: 3.31 (br s, 2 H, Cb C–H), 4.07 (br s, 2 H, Cb C–H), 0.60–3.60 (br m, 6 H, Cb B–H), 6.68 (t, 1 H, pz H), 7.73 (d, 2 H, pz H). ^{11}BNMR (CH_2Cl_2) δ: −18.97, −15.99, −10.76, −9.56, −1.01, 5.49 (B–N). IR (nujol, cm^{-1}): 2590 (s, ν_{B-H}). *meso*-**7b** ^{1}H ($CDCl_3$) δ: 3.30 (br s, 2 H, Cb C–H), 4.00 (br s, 2 H, Cb C–H), 0.80–3.31 (br m, 16 H, Cb B–H), 6.67 (t, 1 H, pz H), 7.75 (d, 2 H, pz H). ^{11}B NMR CH_2Cl_2 δ: −18.97, −14.70, −10.74, −9.01, −0.114, 5.48 (B–N). IR (nujol, cm^{-1}): 2584 (s, ν_{B-H}).

Preparation of *dl*- and *meso*-[μ-$C_3N_2H_3$-(7,9-$C_2B_9H_{10}$)$_2$Ni] (8). A basic solution of **3** (2.00 g, 4.23 mmol) was prepared by addition of the salt to a 40% solution of sodium hydroxide (40 mL). The mixture was then subjected to reduced pressure (20 mm) at ambient temperature for 15 min to remove the triethylamine formed. An excess of $NiCl_2{\cdot}6H_2O$ (2.20 g, 9.22 mmol) was added at 0 °C. The reaction mixture was heated to 100 °C and stirred vigorously for 2 h at this temperature. A dark brown solution formed and persisted upon cooling the reaction to ambient temperature. The mixture was acidified with HCl to neutralize the base, and the nickel complex was extracted with 4 × 200 mL portions of ether. The ether layer was washed with 4 × 50 mL portions of water, and the combined ether washings were dried over anhydrous Na_2SO_4. The ether solvent was removed in vacuo to yield 651.0 mg (39% yield) of brown, crystalline **8**. The product was obtained as a roughly 1:1 mixture of diastereomers and was recrystallized from benzene. The diastereomers were separated to yield the brown *dl*-isomer (**8a**) and green *meso*-isomer (**8b**) by column chromatography using neutral alumina (5 cm × 18 cm column) and a benzene/petroleum ether mixture as the eluate (using a solvent gradient starting at 25:75 vol/vol and ending at 60:40). Both isomers could be recrystallized from benzene. Crystals suitable for an X-ray diffraction experiment were grown by slow evaporation of concentrated benzene/petroleum ether solution. Anal. Calcd for $C_7B_{18}H_{23}N_2Ni$: C, 21.63; H, 5.98; B, 50.07; N, 7.21; N, 15.10. Found: C, 21.94; H, 5.91; B, 49.23; N, 7.38; Ni, 14.59. *dl*-**8a** mp: 297–300 °C dec. ^{1}H ($CDCl_3$) δ: −16.5 (br s, Cb B–H), −7.74 (br s, Cb B–H), 0.90–3.70 (br m, Cb B–H), 0.860 (s, pz H), 6.45 (s, pz H), 15.6 (br s, Cb C–H), 19.1 (br s, Cb C–H). ^{11}B (C_6H_6) δ: −147.4, −101.3, −77.99, −13.47, −8.89, −3.00, 2.90, 40.36, 87.87, 102.4. FAB mass spectrum (mass frag, center of envelope m/e): M^+, 388.00. Calcd for M^+: 388.59. IR (nujol, cm^{-1}): 2583 (s, ν_{B-H}). *meso*-**8b** mp: 298–300 °C dec. ^{1}H ($CDCl_3$) δ: −16.7 (br s, Cb B–H), −8.45 (br s, Cb B–H), 0.91–3.65 (br m, Cb B–H), 0.98 (s, pz H), 6.45 (s, pz H), 15.4 (br s, Cb C–H), 19.2 (br s, Cb C–H). FAB mass spectrum (mass frag, center of envelope m/e): M^+, 389.10. Calcd for M^+: 388.59.

Preparation of *dl*- and *meso*-[μ-$C_3N_2H_3$-(7,9-$C_2B_9H_{10}$)$_2$Cu] (9). A basic solution of **3** (2.00 g, 4.23 mmol) was prepared by addition of the salt to a 40% solution of sodium hydroxide (40 mL). The mixture was then subjected to reduced pressure (20 mm) at ambient temperature for 15 min to remove the triethylamine formed. An excess of $CuSO_4{\cdot}6H_2O$ (2.31 g, 9.22 mmol) was added at 0 °C. The reaction mixture was stirred vigorously, maintaining this temperature for 5 h. A dark purple solution formed and persisted upon warming the reaction to ambient temperature. The sodium salt was metathesized using 1.5 equiv of Me_4NCl. The copper complex was extracted with 4 × 200 mL portions of ether. The combined ether washings were dried over anhydrous Na_2SO_4. The ether solvent was removed in vacuo to result in 694.3 mg (42% yield) of brown, crystalline **9**. The product was obtained as a roughly 1:1 mixture of diastereomers and was recrystallized from benzene. The diastereomers were separated to yield the *dl*-isomer (**9a**) and *meso*-isomer (**9b**) by column chromatography (5 × 24 cm column) using neutral alumina and a benzene/petroleum ether mixture as the eluate. Both isomers could be recrystallized from benzene. A crystal of **9b** suitable for an X-ray diffraction experiment was grown by slow evaporation of concentrated benzene/petroleum ether solution. Anal. Calcd for $C_7B_{18}H_{23}N_2Cu$: C, 71.37; H, 5.90; B, 49.46; N, 7.12; Cu, 16.15. Found: C, 21.50; H, 5.75; B, 50.07; N, 7.06; Cu, 15.65. *dl*-**9a** mp: 265–267 °C dec. ^{1}H ($CDCl_3$) δ: 0.100–3.5 (br s, 16 H, Cb B–H), 2.87 (br s, 2 H, Cb C–H), 3.55 (br s, 2 H, Cb C–H), 6.56 (t, 1 H, pz H), 7.64 (d, 2 H, pz H). ^{11}B (C_6H_6) δ: −20.72, −18.43, −15.01, −13.95, −7.88, −6.60, 1.71 (B–N). FAB mass spectrum (mass frag, center of envelope m/e): M^+, 393.10. Calcd for M^+: 393.44. IR (nujol, cm^{-1}): 2578 (s, ν_{B-H}). *meso*-**9b** mp: 266–269 °C dec. ^{1}H ($CDCl_3$) δ: 0.076–3.49 (br m, 16 H, Cb C–H), 2.85 (br s, 2 H, Cb C–H), 3.55 (br s, 2 H, Cb C–H), 6.55 (t, 1 H, pz H), 7.65 (d, 2 H, pz H). ^{11}B (C_6H_6) δ: −20.72, −18.44, −15.10, −13.96, −7.88, −6.00, 1.74 (B–N). FAB mass spectrum (mass frag, center of envelope m/e): M^+, 392.99. Calcd for M^+: 393.44. IR (nujol, cm^{-1}): 2580 (s, ν_{B-H}).

Preparation of *dl*- and *meso*-[μ-$C_3N_2H_3$-(7,9-$C_2B_9H_{10}$)$_2$Fe] (10). A basic solution of **3** (2.00 g, 4.23 mmol) was prepared by addition of the salt to a 40% solution of sodium hydroxide (40 mL). The mixture was then subjected to reduced pressure (20 mm) at ambient temperature for 15 min to remove the triethylamine formed. An excess of $FeCl_2{\cdot}4H_2O$ (1.83 g, 9.22 mmol) was added at 0 °C. The reaction mixture was heated to 100 °C and stirred vigorously for 2 h at this temperature. A dark red-brown solution formed and persisted upon cooling the reaction to ambient temperature. The iron complex was extracted with 4 × 200 mL portions of ether. The ether layer was washed with 4 × 50 mL portions of water, and the combined ether washings were dried over anhydrous Na_2SO_4. The ether solvent was removed in vacuo to result in 703.1 mg (43% yield) of brown, crystalline **10**. The product was obtained as the *dl* racemate by preparative HPLC on a C_{18} column (41.4 × 250 mm) using 9:1 acetonitrile/0.1% aqueous trifluoroacetic acid (flow rate 10 mL min^{-1}) as the solvent mixture. The isomers could be recrystallized from benzene. A crystal of **10a** suitable for an X-ray diffraction experiment was grown by slow evaporation of concentrated methylene chloride solution. Anal. Calcd for $C_7B_{18}H_{23}N_2Fe$: C, 21.79; H, 6.02; B, 50.44; N, 7.26; Fe, 14.48. Found: C, 21.90; H, 5.94; B, 49.93; N, 7.30; Fe, 14.51. FAB mass spectrum (mass frag, center of envelope m/e): M^+, 386.00. Calcd for M^+: 385.75. *dl*-**10a** mp: 293–294 °C dec. ^{1}H (CD_2Cl_2) δ: −28.1 (br s, Cb C–H), −14.5 (br s, Cb B–H), −10.5 (br s, Cb B–H), −7.02 (br s, Cb B–H), −4.70 (s, pz H), 0.80–3.30 (br m, Cb B–H), 3.59 (s, pz H), 27.8 (br s, Cb C–H). ^{11}B (CH_2Cl_2) δ: −515.1, −462.5, −431.1, −76.46, −13.70, −9.49, 2.28, 9.41, 24.27, 30.3.

Preparation of *dl*- and *meso*-[μ-$C_3N_2H_3$(4-COOH)-(7,9-$C_2B_9H_{10}$)$_2$Co] (11). A basic solution of **4** (0.10 g, 0.22 mmol) was prepared by addition of the complex to a saturated solution of sodium citrate (0.53 g, 1.82 mmol) and by adjusting the pH to 13 by addition of NaOH pellets (0.80 g, 2.00 mmol), and the reaction mixture was stirred vigorously at 100 °C overnight. The mixture was then subjected to reduced pressure (20 mm) at ambient temperature for 15 min to remove the triethylamine formed. Addition of $CoCl_2{\cdot}6H_2O$ (0.21 g, 0.90 mmol) was followed by stirring at ambient temperature for 25 min. A dark yellow solution formed and persisted upon cooling the reaction to ambient temperature. The mixture was acidified with HCl to neutralize the base, and the cobalt complex was extracted with 4 × 20 mL portions of methylene chloride. The organic layer was washed with 4 × 20 mL portions of water, and the combined organic layers were dried over anhydrous Na_2SO_4. The solvent was removed in vacuo to result in 48.2 mg (50% yield) of orange-yellow, crystalline **11**. The product was obtained as a roughly 1:1 mixture of diastereomers containing an impurity, tentatively identified as *closo*-$C_2B_7H_{13}$. Repeated dissolution in ether, filtration, and concentration resulted in removal of the impurity. The sodium salt of the ligand can also be employed in this reaction. ^{1}H NMR ($CDCl_3$/(CD_3)$_2$O) δ: 2.14 (br s, 2 H, Cb C–H *meso*), 2.97 (br s, 2 H, Cb C–H *dl*), 3.34 (br s, 2 H, Cb C–H *meso*), 4.12 (br s, 2 H, Cb C–H *dl*), 8.14 (s, 2 H, pz H *dl*), 8.20 (s, 2 H, pz H *meso*). ^{11}B NMR (ethyl ether) δ: −18.37, −15.24, −13.94, −10.27, −8.92, −8.32, −0.04, 5.86 (B–N), 6.61 (B–N). IR (nujol, cm^{-1}): 3131 (ν_{O-H}), 2528 (ν_{B-H}), 1706 ($\nu_{C=O}$), 1567 ($\nu_{C=O}$). FAB mass spectrum $C_8B_{18}H_{23}N_2O_2Co$ (mass frag, center of envelope m/e): M^+, 433.20. Calcd for M^+: 433.2882. Anal. Calcd for $C_8B_{18}H_{23}N_2O_2Co$: C, 32.54; H, 9.19; B, 47.92; N, 10.35. Found: C, 32.57; H, 9.14; B, 47.54; N, 10.35. The diastereomers were separated to yield *dl*-isomers (**11a**) and a *meso*-isomer (**11b**) by preparative HPLC on a C_{18} column (41.4 × 250 mm) using 9:1 acetonitrile/0.1% aqueous trifluoroacetic acid (flow rate 10 mL min^{-1}) as the solvent mixture with retention times of 17.8 min for **11b** and 25.0 min for **11a**. Both isomers could be recrystallized from a mixture of ethyl acetate and toluene containing a trace of ether. A crystal of **11b** was chosen for an X-ray diffraction experiment. *dl*-**11a** ^{1}H NMR ((CD_3)$_2$O) δ: 3.51 (br s, 2 H, Cb C–H), 4.89 (br s, 2 H, Cb C–H), 8.53 (s, 2 H, pz H). ^{11}B NMR (ethyl ether) δ: −18.08, −15.16, −13.96, −10.15, −8.77, −8.14, 0.21, 5.86 (B–N). IR (nujol, cm^{-1}): 2580 (s), 1735 (sh), 1702 (s), 1565 (m), 1248 (s). *meso*-**11b** ^{1}H NMR ((CD_3)$_2$O) δ: 2.58 (br s, 2 H, Cb C–H), 3.53 (br s, 2 H, Cb C–H), 8.47 (s, 2 H, pz H). ^{11}B NMR (ethyl ether) δ: −18.77, −14.02, −10.31, −0.65, 5.71 (B–N). IR (nujol, cm^{-1}): 2582 (s), 1707 (s), 1570 (m), 1256 (s).

Protocol for the Preparation of Radiolabeled [μ-$C_3N_2H_3$(4-COOH)-(7,9-$C_2B_9H_{10}$)$_2$^{57}Co] (12ab) and Conjugated T84.66 Mab. A. Preparation of 12ab. To 5.5 mCi of ^{57}Co as $CoCl_2$ (7 mCi/μg of Co) in 0.1 N

Table VIII. Details of the Crystallographic Data Collection[a]

	7a	8a	8b	9b	10a	11b
cryst size (mm)	0.34 × 0.28 × 0.40	0.40 × 0.40 × 0.45	0.29 × 0.29 × 0.39	0.39 × 0.39 × 0.45	0.25 × 0.15 × 0.28	0.15 × 0.10 × 0.20
normal to faces	0$\bar{1}$1, 011, 100		012, 01$\bar{2}$, 100	0$\bar{1}$2, 101, 011	100, 011, 0$\bar{1}$1	010, 001, 100
appearance	red-orange parallelepiped	deep red fragment	dark green parallelepiped	deep purple fragment	red parallelepiped	orange plate
space group	$P2_1/c$	$Pnma$	$P2_12_12_1$	$P2_12_12_1$	$P2_1/c$	$P\bar{1}$
a (Å)	10.618 (1)	13.6874 (7)	7.2139 (9)	7.1854 (8)	10.6926 (5)	9.966 (2)
b (Å)	13.366 (1)	15.8587 (8)	13.404 (1)	13.434 (2)	13.3320 (7)	10.475 (2)
c (Å)	14.326 (2)	11.2429 (6)	19.768 (2)	19.980 (2)	14.3288 (7)	17.134 (3)
α (deg)						79.957 (7)
β (deg)	109.925 (3)				110.081 (1)	77.882 (7)
γ (deg)						74.732 (7)
V (Å^3)	1901	2447	1908	1925	1918	1674
Z	4	4 (8 half molecules)	4	4	4	2
ρ(calcd) (g cm^{-3})	1.36	1.28	1.23	1.37	1.34	1.30
μ (cm^{-1})	8.9 (not applied)	8.0 (not applied)	10.1 (not applied)	11.3 (not applied)	7.7 (not applied)	10.0
scan width, below Kα_1	1.3	1.3	1.3	1.3	1.3	1.3
above Kα_2	1.5	1.6	1.6	1.6	1.6	1.6
scan rate (deg min^{-1})	6.0	12.0	3.0	3.0	6.0	3.0
no. of unique reflections	3364	2242	1954	1973	4402	4659
no. of observed ($I > 3\sigma(I)$) reflections	2669	1404	1791	1832	3537	2818
2θ max (deg)	50	50	50	50	55	46
data collected	$+h, +k, \pm l$	$+h, +k, +l$	$+h, +k, +l$	$+h, +k, +l$	$+h, +k, \pm l$	$+h, \pm k, \pm l$
no. of parameters refined	253	103	118	212	253	224
R, R_w, GOF	0.046, 0.064, 2.04	0.067, 0.084, 2.30	0.048, 0.065, 2.23	0.047, 0.059, 2.27	0.034, 0.049, 1.62	0.082, 0.096, 2.44

[a] Conditions: temperature, 298 K; radiation (graphite monochromator), Mo Kα; wavelength, 0.7107 Å.

HCl (ICN Chemical & Radioisotope Division, 30 μL) was added 1.03 mg **4** in 100 μL of 2 N NaOH, and the reaction was stirred in the dark at 50 °C for 15 h. The reaction was cooled to 0 °C and carefully neutralized with 75 μL of 4 N HCl, and ^{57}Co-**9** was isolated by ether extraction (3 × 200 μL). The ether was evaporated in a Speed Vac, and the radiochemical yield was 3.22 mCi (59%).

B. Synthesis of *N*-Hydroxysulfosuccinimide Active Ester of 12ab. To *N*-hydroxysulfosuccinimide (6 μmol in 20 μL, 0.2 M pyridine/HCl, pH 5.2) and 1-ethyl-3-(3-(dimethylamino)propyl)carbodiimide hydrochloride (6 μmol in 20 μL of 0.2 M pyridine/HCl, pH 5.2) was added **12ab** (3.22 mCi), in 80 μL of acetonitrile (HPLC grade), and the reaction was stirred under vortex at room temperature for 1 h. The active esters of **12ab** were purified by reversed-phase HPLC on a 2.1 × 30 mm C_8 column using a trifluoroacetic acid/acetonitrile solvent system. The purification was monitored at 280 nm, and the diastereomeric active esters of **12ab** eluted as a doublet at ca. 85% acetonitrile. The radiochemical yield was 1.99 mCi (62%).

C. Conjugation of Anti-CEA MAb T84.66 with the Active Esters of 12ab. Anti-CEA Mab T84.66 produced by Damon Biotech was first chromatographed at 0.2 mL min^{-1} on a 1 × 60 cm Superose 12 gel filtration column equilibrated with 0.1 M HEPES, pH 8.5. To 5 g of T84.66 in 1 mL of 0.1 M HEPES, pH 8.5, was added 1.99 mCi of the **12ab** active esters from above, and the conjugation reaction was stirred at room temperature for 1 h. The **12ab**–T84.66 conjugate was chromatographed at 0.2 mL min^{-1} on a 1 × 30 cm Superose 12 column equilibrated with 0.05 M Na_2PO_4, 0.15 M NaCl, pH 8.0. The purification was monitored at 280 nm. Labeled T84.66 eluted in 3.44 min with a radiochemical yield of 0.52 mCi (26%).

General Methods of Crystallographic Analyses. All data were collected on automated diffractometers in the θ–2θ scan mode with Mo K$_\alpha$ radiation. Data for **8a**, **8b**, **9b**, **10a**, and **11b** were collected on a Huber diffractometer constructed by Professor C. E. Strouse of this department. Data for **7a** was collected on a Picker FACS-1 modified by Professor C. E. Strouse. All calculations were performed using the DEC VAX 11/750 computer of the J. D. McCullough Crystallographic Laboratory and the UCLA crystallographic programs. Data were corrected for Lorentz and polarization effects. Programs used in this work include locally modified versions of the following programs: CARESS (Broach, Coppens, Becker, and Blessing), peak profile analysis, Lorentz and polarization corrections, ORFLS (Busing, Martin, and Levy), structure factor calculation and full-matrix least-squares refinement, SHELX76 (Sheldrick) crystal structure package, and ORTEP (Johnson). All structures were solved with use of heavy-atom methods unless otherwise noted. Remaining atoms were located by use of difference electron density maps. In the course of refinement, all cage C and B atoms were initially assigned scattering factors for boron. After refinement, carboranyl carbon atom positions could be distinguished by their anomalously low temperature factors and by shorter interatomic distances. Reported R and R_w values are defined as $R = [\sum(|F_o| - |F_c|)/\sum|F_o|]$ and $R_w = [\sum w(|F_o| - |F_c|)^2/\sum w|F_o|2]^{1/2}$, where $w = 1/\sigma^2(F_o)$ and "goodness of fit" is defined by $[\sum w(|F_o| - |F_c|)^2/(N_{obsd} - N_{variable})]^{1/2}$. Scattering factors for hydrogen were obtained from Stewart et al.,[36] and those for other atoms were taken from ref 37. Details of the individual data collections are given in Table VIII.

X-ray Crystallographic Analysis of 7a. A red-orange crystal, obtained from a methylene chloride solution, was mounted on a glass fiber. Data were collected to a maximum 2θ = 50° at 145 K. All atoms were located by use of statistical methods (MULTAN 80). All non-hydrogen atoms were refined anisotropically. All hydrogen atoms were included in located positions and were assigned an arbitrary temperature factor (B) of 5.0 Å^2. Anomalous dispersion terms were applied to the scattering of Co. Both isomers of the racemate are present in the crystal. Least-squares refinement converged to R = 0.046 and R_w = 0.064. The maximum and minimum peaks on a final difference electron density map were 0.6 eÅ^{-3}. Final positional and thermal parameters are listed in Tables S.3 and S.4 as supplementary material.

X-ray Crystallographic Analysis of 8a·C_6H_6. A red-brown crystal, obtained from a benzene solution, was mounted on a glass fiber. Data were collected to a maximum 2θ = 50° at 25 °C (298 K). A mirror plane passes through Ni, C3B, and H3B as well as through a molecule of benzene. Although this isomer is known not to have mirror symmetry, the disorder found in positions 1, 3, 7, and 11 is not unprecedented. All of these positions were refined with half boron/half carbon occupancy with u values as well as positional values kept equal for each pair of occupants. Anisotropic parameters were refined for Ni atoms, C and N atoms of the pyrazole fragment, and three C atoms of the benzene. All other non-hydrogen atoms were refined isotropically. Hydrogen atoms of the benzene molecule were kept in calculated positions with u assigned as 0.15 Å^2. All other hydrogens were kept in located positions and were assigned u = 0.065 Å^2. Anomalous dispersion terms were applied to the scattering of Ni. Both isomers of the racemate are present in the same location in the crystal. Least-squares refinement converged to R = 0.067 and R_w = 0.084. The maximum and minimum peaks on a final difference electron density map were 0.2 eÅ^{-3}. Final positional and thermal parameters are listed in Tables S.3 and S.4 as supplementary material.

X-ray Crystallographic Analysis of 8b. A dark green crystal suitable for an X-ray crystallographic study was grown from a petroleum ether solution and mounted on a glass fiber. Data were collected to a maximum 2θ = 50° at 298 K. The Ni atom was refined anisotropically, and the remaining non-hydrogen atoms were refined isotropically. The positions of all hydrogens were located and assigned an arbitrary tem-

(36) Stewart, R. F.; Davidson, E. R.; Simpson, W. T. *J. Chem. Phys.* **1965**, *42*, 3175.
(37) International Tables for X-ray Crystallography; Kynoch Press: Birmingham, England, 1974; Vol. IV.

perature factor (B) of 3.5 Å^2. Anomalous dispersion terms were applied to the scattering of Ni. The molecule is diastereomeric, and only one isomer is present in the crystal. Least-squares refinement converged to $R = 0.050$ and $R_w = 0.067$. The maximum and minimum peaks on a final difference electron density map were 0.4 eÅ^{-3}. Final positional and thermal parameters are listed in Tables S.3 and S.4 as supplementary material.

X-ray Crystallographic Analysis of 9b. A deep purple crystal suitable for an X-ray crystallographic study was grown from a methylene chloride solution and mounted on a glass fiber. Data were collected to a maximum $2\theta = 50°$ at 298 K. The position of the Cu atom was obtained from the Patterson synthesis. All remaining atoms, including hydrogen atoms, were located in subsequent difference Fourier maps. The Cu atom and non-hydrogen atoms of the pyrazole fragment were refined anisotropically, and the remaining non-hydrogen atoms were refined isotropically. The positions of all hydrogens were located, refined, and assigned an arbitrary temperature factor (B) of 3.0 Å^2. Anomalous dispersion terms were applied to the scattering of Cu. The molecule is diastereomeric, and only one isomer is present in the crystal. Least-squares refinement converged to $R = 0.055$ and $R_w = 0.071$. The maximum and minimum peaks on a final difference electron density map were 0.8 eÅ^{-3}. Final positional and thermal parameters are listed in Tables S.3 and S.4 as supplementary material.

X-ray Crystallographic Analysis of 10b. A deep red crystal suitable for an X-ray crystallographic study was grown from a methylene chloride solution and mounted on a glass fiber. Data were collected to a maximum $2\theta = 50°$ at 298 K. The Fe atom and all the other non-hydrogen atoms were refined anisotropically. The positions of all hydrogens were located and assigned u values of 0.05 Å^2. Anomalous dispersion terms were applied to the scattering of Fe. Both isomers of the racemate are present in the crystal. Least-squares refinement converged to $R = 0.034$ and $R_w = 0.049$. The maximum and minimum peaks on a final difference electron density map were 0.3 eÅ^{-3}. Final positional and thermal parameters are listed in Tables S.3 and S.4 as supplementary material.

X-ray Crystallographic Analysis of 11b·2C$_6$H$_5$CH$_3$. An orange crystal suitable for an X-ray crystallographic study was grown from an ethyl acetate/toluene solution and mounted on a glass fiber. Data were collected to a maximum $2\theta = 50°$ at 298 K. The Co atom, two oxygen atoms of the carboxylic acid fragment, and the C atoms of a toluene solvate were refined anisotropically, and all other atoms were refined isotropically. One of the toluene molecules exhibited disorder about a center of symmetry. Methyl hydrogens for the ordered toluene molecule were included in calculated positions as members of a rigid group: C–H = 1.0 Å, H–C–H = 109.5°, $u = 0.15$ Å^2. No hydrogen atoms were included for the disordered toluene molecule. All phenyl rings were included as rigid, kept in located positions, $u = 0.089$ Å^2. Anomalous dispersion terms were applied to the scattering of Co. The molecule is diastereomeric, and only one isomer is present in the crystal. Least-squares refinement converged to $R = 0.082$ and $R_w = 0.096$. The maximum and minimum peaks on a final difference electron density map were 0.23 eÅ^{-3}. Final positional and thermal parameters are listed in Tables S.3 and S.4 as supplementary material.

Acknowledgment. We thank the National Institutes of Health for support of this research under Grants RO1–CA 31753 and PO1-CA 43904. S.E.J. gratefully acknowledges the National Science Foundation for support from a NSF postdoctoral fellowship (CHE90-01819). F.A.G. gratefully acknowledges the NIH for support from a MARC NIH predoctoral fellowship (GM11586).

Supplementary Material Available: Tables of bond distances and angles, positional and equivalent isotropic thermal parameters, and anisotropic thermal parameters, and details of the crystallographic data collection (51 pages); tables of observed and calculated structure factors (72 pages). Ordering information is given on any current masthead page.

Mechanisms of Cage Reactions: Kinetics of Combination and Diffusion after Picosecond Photolysis of Iron(II) Porphyrin Ligated Systems

Teddy G. Traylor,* Douglas Magde,* Jikun Luo, Kevin N. Walda, Debkumar Bandyopadhyay, Guo-Zhang Wu, and Vijay S. Sharma

Contribution from the Department of Chemistry, University of California, San Diego, 9500 Gilman Drive, La Jolla, California 92093-0506. *Received November 22, 1991. Revised Manuscript Received June 29, 1992*

Abstract: The kinetics of transient absorption changes for a number of protoheme–ligand systems after subpicosecond photolysis have been investigated. When the photolyzed ligand is *tert*-butyl, pentachlorophenyl, pentafluorophenyl, 5α-cholestan-3α-yl, or 5α-cholestan-3β-yl isocyanide or 1-methylimidazole, a concentration-independent relaxation is observed. Its decay is accurately exponential. Therefore the geminate pair created by photolysis disappears in a clear first-order process and does not follow the power law kinetics reported for similar systems with other ligands in high-viscosity solvents or in glasses at low temperatures. Proteins combining with isocyanides also show exponential geminate recombination with a rate constant of $\sim 10^{11}$ s^{-1}, which is very close to that of the model systems. Geminate return of carbon monoxide to 1-methylimidazole–protoheme in glycerol is much slower (3×10^9 s^{-1}) but is also almost exponential.

Introduction

Reactions in which combination of reaction partners is competitive with diffusive separation have been treated with two distinct mechanistic theories[1-8] which emphasize either the statistical diffusion of the two nonattractive partners through the solvent or activation-controlled passage through a series of distinct (e.g. solvation) states of different energies. In either case, we might represent the process as shown in eq 1, where the vertical lines

(1) Smoluchowski, M. V. *Z. Phys. Chem.* **1917**, *92*, 129.
(2) Noyes, R. M. *Prog. React. Kinet.* **1961**, *1*, 129.
(3) (a) Collins, F. C.; Kimball, G. E. *J. Colloid Sci.* **1949**, *4*, 425. (b) Olea, A. F.; Thomas, J. K. *J. Am. Chem. Soc.* **1988**, *110*, 4494.
(4) Frauenfelder, H.; Wolynes, P. G. *Science* **1985**, *229*, 337.
(5) (a) Karim, O. A.; McCammon, J. A. *J. Am. Chem. Soc.* **1986**, *108*, 1762. (b) Ciccotti, G.; Ferrario, M.; Hynes, J. T.; Kapral, R. *J. Chem. Phys.* **1990**, *93*, 7137.
(6) Alwattar, A. H.; Lumb, M. D.; Birks, J. B. In *Organic Molecular Photophysics*; Birks, J. B., Ed.; Wiley: New York, 1973; Vol. 1, 403.
(7) Rice, S. A. In *Comprehensive Chemical Kinetics*; Bamford, C. H., Compton, R. G., Eds.; Elsevier: New York, 1985; Vol. 25.
(8) (a) Winstein, S.; Clippinger, E.; Fainberg, A. H.; Robinson, G. C. *J. Am. Chem. Soc.* **1954**, *76*, 2597. (b) Winstein, S.; Klinedinst, P. E., Jr.; Robinson, G. C. *J. Am. Chem. Soc.* **1961**, *83*, 885. (c) Winstein, S.; Klinedinst, P. E., Jr.; Clippinger, E. *J. Am. Chem. Soc.* **1961**, *83*, 4986. (d) Winstein, S.; Robinson, G. C. *J. Am. Chem. Soc.* **1958**, *80*, 169 and related papers. For reviews see: (e) Harris, J. M. *Prog. Phys. Org. Chem.* **1974**, *11*, 89. (f) Szwarc, M., Ed. Ions and Ion Pairs in Organic Reactions; Wiley-Interscience: New York, 1974; Vol. 2, Chapter 3, p 247 ff.

0002-7863/92/1514-9011$03.00/0